Gain improvement for the THz p-Ge laser using neutron transmutation doped active crystal

E. S. Flitsiyan,[a,*)] M. V. Dolguikh,[a)] A. V. Muravjov,[a)] E. W. Nelson,[a)] T. W. Du Bosq,[a)] R. E. Peale,[a,] C. J. Fredricksen,[b)] W. G. Vernetson,[c)]

[a)] Department of Physics, University of Central Florida, Orlando FL, 32816. [b)] Zaubertek, Inc. 1809 E. Broadway St. #313 Oviedo FL 32765. [c)] Department of Nuclear and Radiological Engineering, University of Florida, Gainesville FL, 32611. [*)]esf@physics.ucf.edu

ABSTRACT

A far-infrared p-type germanium laser with active crystal prepared from ultra pure single-crystal Ge by neutron transmutation doping (NTD) is demonstrated. Calculations show that the high uniformity of Ga acceptor distribution achieved by NTD significantly improves average gain. The negative factor of stronger ionized impurity scattering due to high compensation in NTD Ge is shown to be unremarkable for the gain at moderate doping concentrations sufficient for laser operation. Experimentally, this first NTD laser is found to have lower current-density lasing threshold than the best of a number of melt-doped laser crystals studied for comparison.

INTRODUCTION

Terahertz p-Ge lasers operate on intra-valence-band transitions in bulk p-type doped germanium crystals. They remine a most powerful semiconductor lasers in that frequency range, though there are some disadvantages in comparison with recently developed quantum cascade lasers. These are low efficiency and fast overheating, which result in inability of continuous wave operation and requirements of liquid helium cooling. The main reason of these limitations is low small signal gain (< 0.1 cm^{-1}).[1] One of the important factors responsible for a low gain in p-Ge lasers is ununiform doping of the laser crystals.

Active p-Ge laser crystals are traditionally Ga-doped during melt growth. Room temperature resistivity variations typically exceed 4 – 10 % over both macroscopic (cm) and microscopic (sub-mm) length scales.[2] In the lightly-doped ~ 35 Ω-cm material required for p-Ge lasers, intrinsic carriers significantly contribute to the room temperature resistivity. Hence, actual variations in acceptor concentration can be much higher than the reported room temperature resistivity variations.

This paper presents results of neutron transmutation doping (NTD) [2-4] to produce uniformly doped p-Ge laser material. Some preliminary results have been reported in.[5,6] Room temperature resistivity variations of NTD Ge over sub-mm to cm lengths are less than 0.7%.[2] The NTD method immerses undoped Ge in neutron flux of a nuclear reactor. Three of the five stable natural Ge isotopes, ^{70}Ge, ^{74}Ge and ^{76}Ge (Table 1) are transmuted by thermal neutrons into ^{71}Ga (shallow acceptor), ^{75}As (shallow donor), and ^{77}Se (double donor), respectively. The remaining two isotopes, Ge^{72} and Ge^{73}, transmute into other stable Ge isotopes, Ge^{73} and Ge^{74}, respectively in according to the following nuclear reactions (Table 2) and scheme of decay in Figs. 1-3.

Table I. The Natural Abundance of Germanium Isotopes

Isotope	Abundance	Isotope	Abundance	Isotope	Abundance
Ge^{70}	20.65%	Ge^{73}	7.86%	Ge^{76}	7.72%
Ge^{72}	27.43%	Ge^{74}	36.34%		

The possible lattice defects (vacancies and amorphous regions) introduced by fast neutrons from the reactor neutron flux can be removed by annealing.

The concentration of impurities N in the NTD method is proportional to the thermal neutron flux Φ, nuclear reaction cross section σ_i for the given isotope and its abundance θ_i in the given isotope mixture, according

Terahertz for Military and Security Applications II, edited by R. Jennifer Hwu, Dwight L. Woolard, Proceedings of SPIE Vol. 5411 (SPIE, Bellingham, WA, 2004)
0277-786X/04/$15 · doi: 10.1117/12.542695

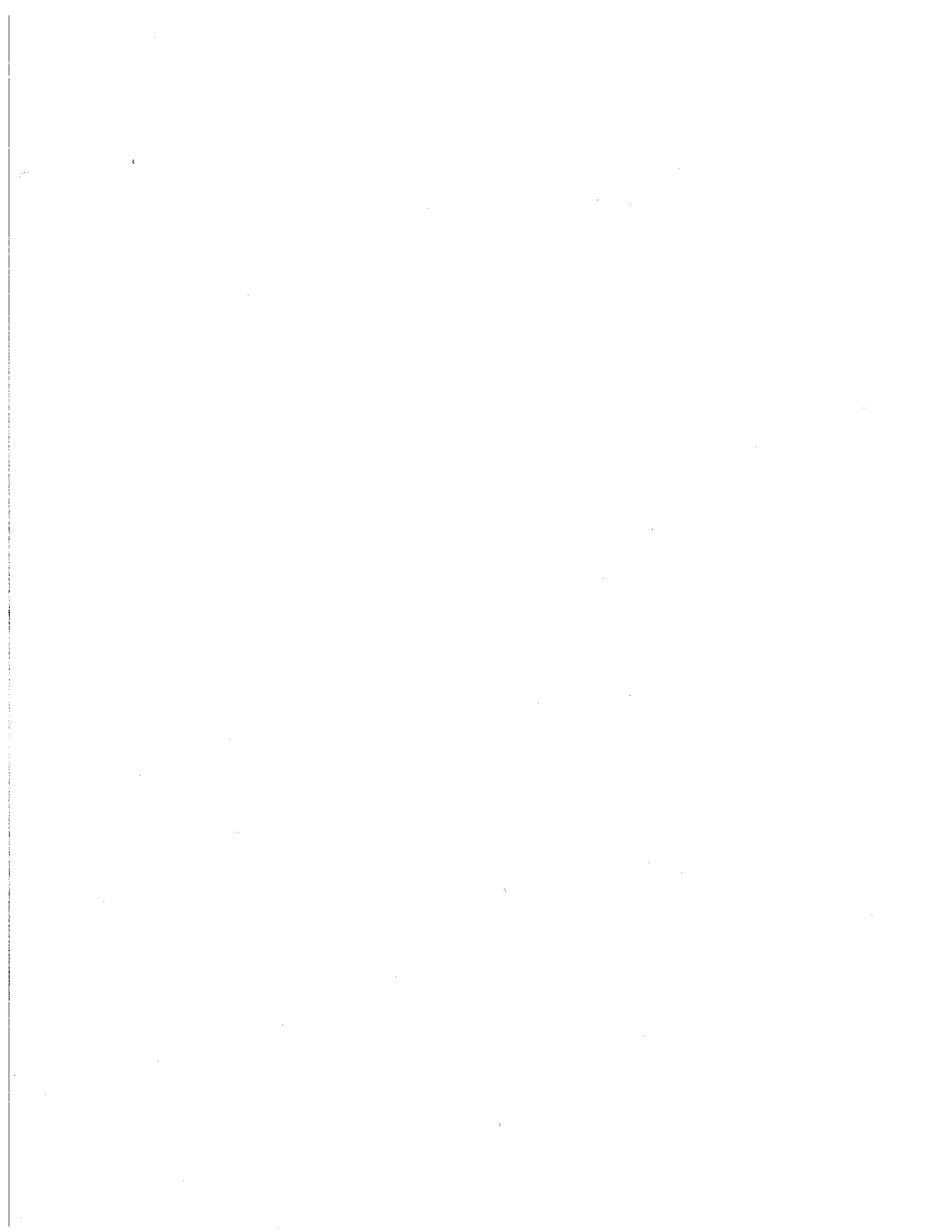

to N = $\theta_i \sigma_i \Phi$. Considering that the values of σ_i lie in the 10^{-23} - 10^{-24} cm^{-2} range, large neutron fluences are required to transmute a significant number of atoms of one element into another. With the thermal neutron fluences available in modern nuclear reactors one can dope Ge up to the metal-insulator transition. Much lower acceptor concentrations in the range 10^{13} to 10^{14} cm^{-3} are needed for p-Ge lasers. The concentrations of transmuted elements in Ge as a function of neutron fluence are shown in Fig. 4.

Table 2. Possible Nuclear Transitions in Ge isotopes. Most of the product isotopes are unstable and decay into stable isotopes of Ga, As, and Se.

Isotope	Nuclear reaction	Limit energy of reaction (Mev)	Cross section (mbarn)	Half-life of product isotope
^{70}Ge	$^{70}Ge(n,\gamma)^{71}Ge$	-7.52	3420±350 (thermal neutrons)	12.5d
	$^{70}Ge(n,2n)^{69}Ge$	11.70	6 60±230 (fission spectra neutrons)	1.6d
	$^{70}Ge(n,3n)^{68}Ge$	20.59	1.5*10^{-5} (fast neutrons)	288d
	$^{70}Ge(n,p)^{70}Ga$	0.88	129 (fast neutrons)	21.4 m
^{72}Ge	$^{72}Ge(n,\gamma)^{73}Ge$	-6.88	-	Stable
	$^{72}Ge(n,2n)^{71}Ge$	10.90	640 (fast neutrons)	12.5d
	$^{72}Ge(n,p)^{72}Ga$	3.26	<0.01	14.12h
	$^{72}Ge(n,\alpha)^{69}Zn$	-1.5	0.020±0.005	13.5h
^{73}Ge	$^{73}Ge(n,3n)^{71}Ge$	17.78	2.7*10^{-4} (fission spectra neutrons)	12.5d
	$^{73}Ge(n,p)^{73}Ga$	0.78	137±69 (fast neutrons)	4.85h
^{74}Ge	$^{74}Ge(n,\gamma)^{75}Ge$	-6.58	40±8 (thermal neutrons)	1.37h
	$^{74}Ge(n,\gamma)^{75m}Ge$			49sec
	$^{74}Ge(n,p)^{74}Ga$	4.78	41 (fast neutrons)	7.8 min
^{76}Ge	$^{76}Ge(n,\gamma)^{77}Ge$	-6.10	115±25	11.3h
	$^{76}Ge(n,2n)^{75}Ge$	9.57	1800 (fast neutrons)	1.37h

The low doping levels needed for p-Ge lasers require less than 1 hour irradiation in a typical reactor. The donors As and Se are produced in lower concentrations than the acceptor Ga, so that NTD Ge is p-type with reported compensations $K = N_d/N_a$ in the range 0.32 – 0.40,[3,4] where $N_{d(a)}$ is the concentration of donors (acceptors). In the few melt-doped p-Ge lasers tested for compensation, the value has been between[7] 0.07 and[8] 0.3 but the maximum allowable compensation for a p-Ge laser is uncertain.

A practical consideration in favor of the NTD process for producing p-Ge lasers is that the ultra-pure starting material is readily available from commercial suppliers. Large single crystals of this highly-refined germanium are used in gamma-ray detectors. In contrast, suitable melt-doped p-Ge is not a standard item of commerce.

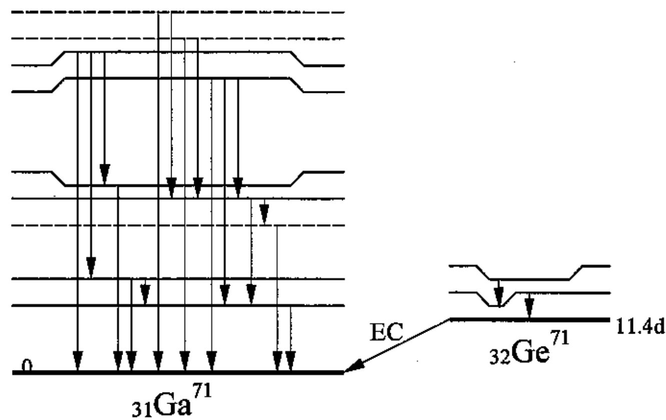

Fig. 1. Nuclear level properties of ^{71}Ge. ^{71}Ge decays into stable ^{71}Ga by electron capture.

Long lived radioactivity can be generated in natural germanium only by activation of impurities, since final transmutation products of natural Ge isotopes are stable and result from rapid decays. Most of the expected impurities in ultra-pure Ge starting material generate isotopes with half-lives from seconds to minutes. Pre-irradiation polishing with diamond ensures that residual surface impurities are mainly carbon. Diamond powder may contain Zn as a (removable) impurity, which can lead to radioactive Zn-65. Cleaning of cut laser rods in HF vapor removes surface contamination without introducing new metal ions.

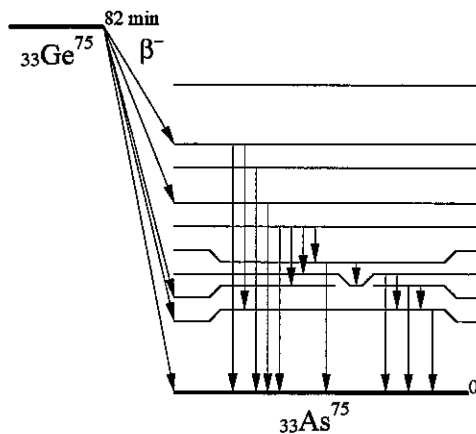

Fig. 2. Nuclear structure of ^{75}Ge. β-decay leads to formation of the stable ^{75}As isotope.

THEORY

The mechanism of p-Ge lasing is based on direct optical transitions between light and heavy-hole valence subbands at liquid-helium temperatures in crossed electric and magnetic fields.[1] Measured values of gain ranges from 0.01 to 0.1 cm^{-1},[1] but these are considerably lower than predicted by recent simulations [9], which give a maximum theoretical stimulated emission cross-section of 2×10^{-15} cm^2. For active p-Ge with usual maximum hole concentration of $\sim 2 \times 10^{14}$ cm^{-3}, this corresponds to a gain of 0.4 cm^{-1}. A probable cause of the observed low gain is field inhomogeneity within the active crystal. Breaking the condition of exact electric and magnetic field orthogonality allows E to have a component parallel to B. Such an E-field component accelerates trapped light

holes in the direction of B until they scatter on optical phonons, decreasing the light-hole lifetime and therefore gain. A deviation from perpendicularity of applied fields by only 1 deg causes a remarkable reduction of gain.[1] Hence field non-uniformity would allow gain as high as the theoretical limit to exist only locally, with losses that must be overcome elsewhere in the medium, giving low values for the observed average gain.

The magnetic field, usually created by a superconducting solenoid or permanent-magnet assembly,[1] is quite uniform within the active crystal. The E-field uniformity, on the other hand, is degraded under non-linear conduction conditions by space and surface charge, which appear due to Hall effect, anisotropic conductivity, and non-uniform doping. Choosing proper orientation of an active crystal eliminates E components parallel to B that are caused by Hall effect and anisotropy. These effects are predictable and well investigated. However, the additional factor that affects E-field uniformity, the non-uniform spatial distribution of acceptors in the crystal, is uncontrollable in a given laser rod.

It is important to emphasize that due to nonlinear J(E) behavior, even moderate doping inhomogeneity dramatically disrupts the electric field homogeneity within the active sample. This drastically reduces the gain because of its strong sensitivity to deviation in angle between local-electric and applied-magnetic fields from 90 degrees. To obtain quantitative estimates of this effect, the internal E-field distribution was found by numerically solving div(J) = 0 using the finite element method. A simple ad hoc model of the non-Ohmic current in the near-saturation regime that qualitatively gives the correct dependence is $J = \sigma E^{(1-s)}$, with saturation factor s = 0.75. Effects of the B-field on current redistribution were neglected. A Gaussian doping anomaly was assumed, $N_a = N_{a0}(1 - b \exp(-r^2 / R^2))$, where b is the degree and R the scale of the anomaly, which might also be a function of direction. The calculated E-field redistribution was combined with gain versus E-field-deviation results from our Monte-Carlo simulation[9] to determine the spatial gain distribution near the anomaly. Gain and doping profiles, such as presented in the Fig. 5 inset, were obtained from straight one dimensional sections of the three dimensional distributions. The dependence of the minimum gain on degree of anomaly b is presented in Fig. 5. These results are valid for any anomaly scale starting from light hole mean free path (10 μm) to the full size of the active crystal.

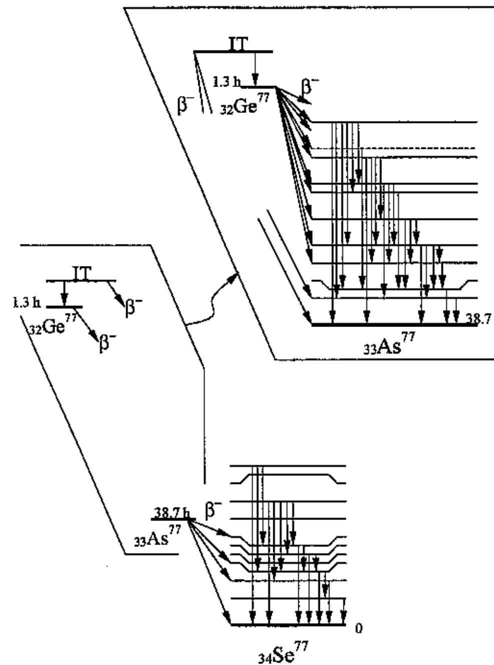

Fig. 3. ^{77}Ge decays from the metastable state via an isomeric transition into the intermediate nuclei of ^{77}As, which then decays into stable ^{77}Se.

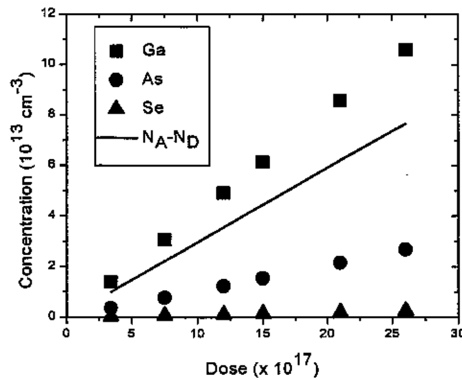

Fig. 4. The concentration of transmuted elements in Ge as a function of neutron dose.

Although the *average* gain reduction will depend on details of the acceptor distribution, the Fig. 5 dependence is characteristic of the effect of non-uniform doping. The region with degraded gain always has a much larger spatial extent than the doping anomaly. For melt-doped p-Ge with just 15% doping inhomogeneity, the gain in certain regions drops 3-fold. These considerations explain the observed performance variations for different crystals cut from the same melt-doped boule, which will be demonstrated below.

Monte Carlo simulation[9] provides predictions for the effect of compensation on gain. Simulation results are presented in Fig. 6, where gain at 100 cm^{-1} is plotted vs. compensation for 4 different hole concentrations. (These Monte Carlo calculations differ from[10] by assuming isotropic dispersion and implementing a more accurate approach to impurity and electron-electron scattering. Thus the gain values in Fig. 6 are smaller than found in [10], where a maximum gain of 0.4 cm^{-1} was calculated.) At zero compensation, the hole concentration that maximizes the gain is 10^{14} cm^{-3}, which is close to the experimental value of $\sim 7 \times 10^{13}$ cm^{-3} .[1] The effect of compensation is in all cases to lower the gain, but this effect becomes less and less pronounced with decreasing hole concentration. At the concentration 3.6×10^{13} cm^{-3}, the effect of compensation is almost negligible.

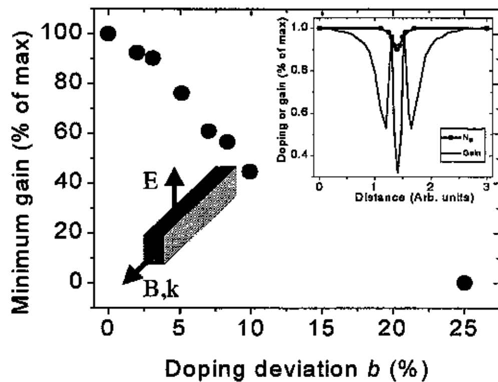

Fig. 5. Simulation of gain cross section at 100 cm^{-1} vs. maximum doping anomaly. Lower inset: A schematic of laser crystal with orientation of applied fields (E, B) and direction of laser output (k). Upper inset: Doping anomaly and gain profiles.

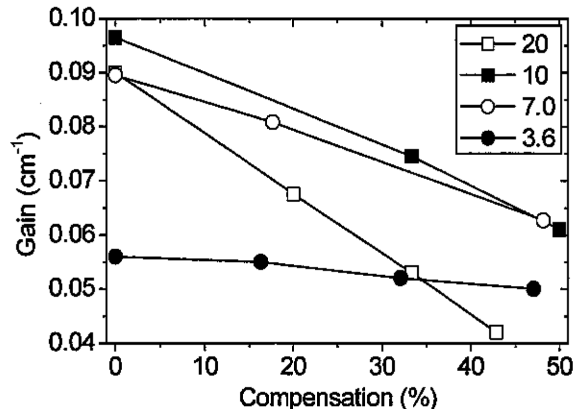

Fig. 6. Monte Carlo calculation of gain cross section at 100 cm^{-1} vs compensation for different hole concentration. The legend gives hole concentration in units $10^{13}cm^{-3}$. Simulation parameters were $E = 1.25kV/cm$, $B = 1T$, and $T = 10$ K.

A complementary measure of p may be deduced from the low temperature saturated current density according to

$$J_s = e\, v_s\, p, \tag{5}$$

where v_s is the average saturated hot hole velocity in Ge at liquid helium temperature. A value of $v_s = 0.98 \times 10^5$ m/s was determined by Monte Carlo simulation with applied fields E = 1 kV/cm and B = 0. Compensation K is related to p and N_a by

$$p = (N_a - N_d) = N_a (1-K) \tag{6}$$

An indication of doping homogeneity is saturation current behavior at high electric field, where the dominant scattering mechanism is optical phonon scattering. Simulated saturation curves (Monte Carlo method[14]) are presented in Fig. 7 for homogeneous and inhomogeneous crystals. The latter is a rather extreme case, where the crystal length L is divided into two sections, one of length 0.9 L and concentration p, and one with length 0.1 L and concentration 0.7 p. The inhomogeneous curve was obtained using the average carrier velocity vs. electric field, obtained from the Monte Carlo simulation in the homogeneous case, together with the continuity condition for current. The transition between ohmic and saturated regions is sharper for the homogeneous crystal.

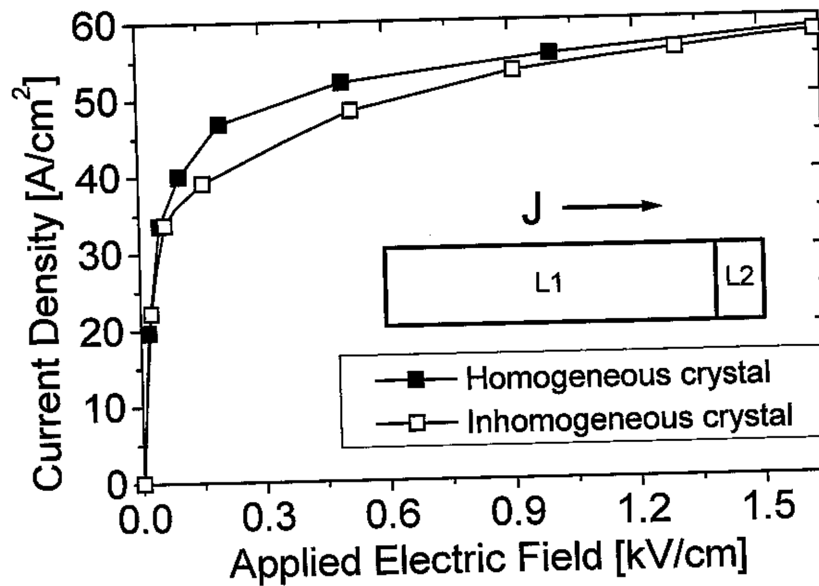

Fig. 7. Monte Carlo calculation of current density as a function of applied electric field for a homogeneous and an inhomogeneous crystal. Inhomogeneity distribution and direction of current are shown schematically in the inset. The total impurity concentration was taken to be $N_i = 6.7 * 10^{13} cm^{-3}$ with 30% compensation ($p = N_a - N_d \sim 3.6 \times 10^{13}$ cm^{-3}).

EXPERIMENT

To determine the statistical dispersion of laser performance resulting from random doping anomalies, 18 laser rods were prepared from Ge melt-doped with Ga, designated material C. The original boule was 9.9 cm in length with 3.4 cm diameter. The vendor (Tydex, St. Petersburg, Russia) specified the axial orientation as [110], the range of resistivity as 34 to 46 Ohm-cm, and the dislocation density as 1000 cm^{-2}. The radial crystallographic orientations were determined by HeNe laser light scattering from suitably etched surfaces.[16] The boule was cross cut into two cylinders of length 46.4 mm and 52.4 mm using a wire saw. These cylinders were then cut in half longitudinally. A low-speed diamond saw then cut the longer hemi-cylinder into nine laser rods (C1-C9), as shown

in Fig. 8. Nine more laser rods (C10-C18) were cut from the shorter hemi-cylinder. Table 3 lists dimensions of the laser rods studied.

Laser cavities were formed using $SrTiO_3$ mirrors attached to the active sample end faces. The back mirror covered one face of the active crystal. The output mirror on the opposite face was of smaller area to allow radiation to escape around the mirror edge. E-field pulses of 1-2 μs duration were generated in the laser crystal by applying high voltage with a thyratron pulser to Ohmic contacts on lateral surfaces of the crystal. Current through the active crystal was monitored using a fast current probe (Pearson 411). The magnetic field was supplied by a superconducting solenoid in Faraday configuration. Laser emission was detected using a Ge:Ga photoconductor immersed in liquid helium at 4 K in the same dewar.

For neutron transmutation doping, a rod was cut from high purity germanium (Perkin Elmer). The electrically-active impurity concentration was specified as 1.02×10^{11} cm^{-3}. The rod was rinsed in spectroscopy-grade acetone, etched in HF vapor, and finally rinsed in distilled water to remove trace surface contaminants. The rod was wrapped in polyethylene and irradiated in the central vertical port of the University of Florida Training Reactor (UFTR, 1.5×10^{12} n/cm^2-sec thermal neutron flux) for 25 minutes.

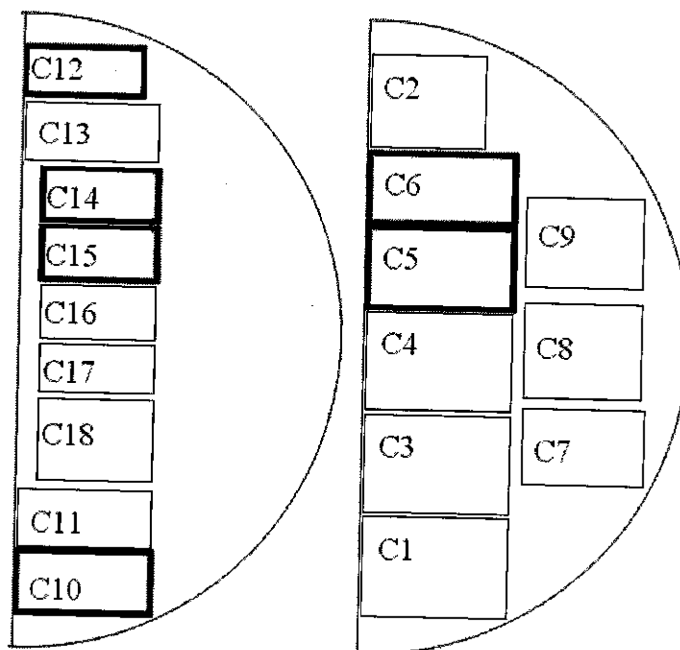

Fig. 8. Crystals cut from a commercial p-Ge boule of melt-doped material C. The crystal cross sections are shown to scale and labeled with their Table 3 designations. The best performers (lowest E-field thresholds) are highlighted.

After irradiation, radionuclides present in the rods were identified using a high purity germanium detection system. Total emission rate was determined with a Geiger counter (Ludlum-3). Seven days after irradiation at UFTR, the radionuclides detected by γ-emission spectroscopy were primarily Ge-77, Ge-75, and As-77. Fourteen days after irradiation, only As-77 was detectable. At that time, the germanium was found to emit ~ 0.01 mR/hr, which is indistinguishable from background.

The NTD rods were tested for laser action before and after annealing. For initial laser testing, the NTD sample measured approximately 37 x 6 x 5 mm^3. This crystal was then cut into four parts measuring 18.38 x 6.16 x 2.44 mm^3 and tested again for lasing prior to annealing. Crystal (D1) was annealed (30 min), re-polished to a final length of 17.40 mm, and tested for laser emission.

Values for p were determined from the saturated current density according to Eq. (5). Comparison of p vs. gallium concentration from neutron activation analysis then provides information about compensation K, according to Eq. (6).

To compare the shape of current saturation curves, two identically shaped rods of NTD and melt materials were immersed in liquid helium and subjected to μs current pulses along their long axis [110]. The experiments were performed in the presence of a small magnetic field (0.19 T) applied axially.

RESULTS

Laser generation zones in the space of applied E and B fields for melt-doped samples C1-C12 and C14-C17 are presented in Fig. 9. Samples C13 and C18 failed repeatedly to produce laser emission, while all other C crystals worked during their first trials. A large variation in electric field threshold is observed. Crystal C6 has the lowest electric field and current density thresholds. The latter has the value 74.4 A/cm^2 for C6.

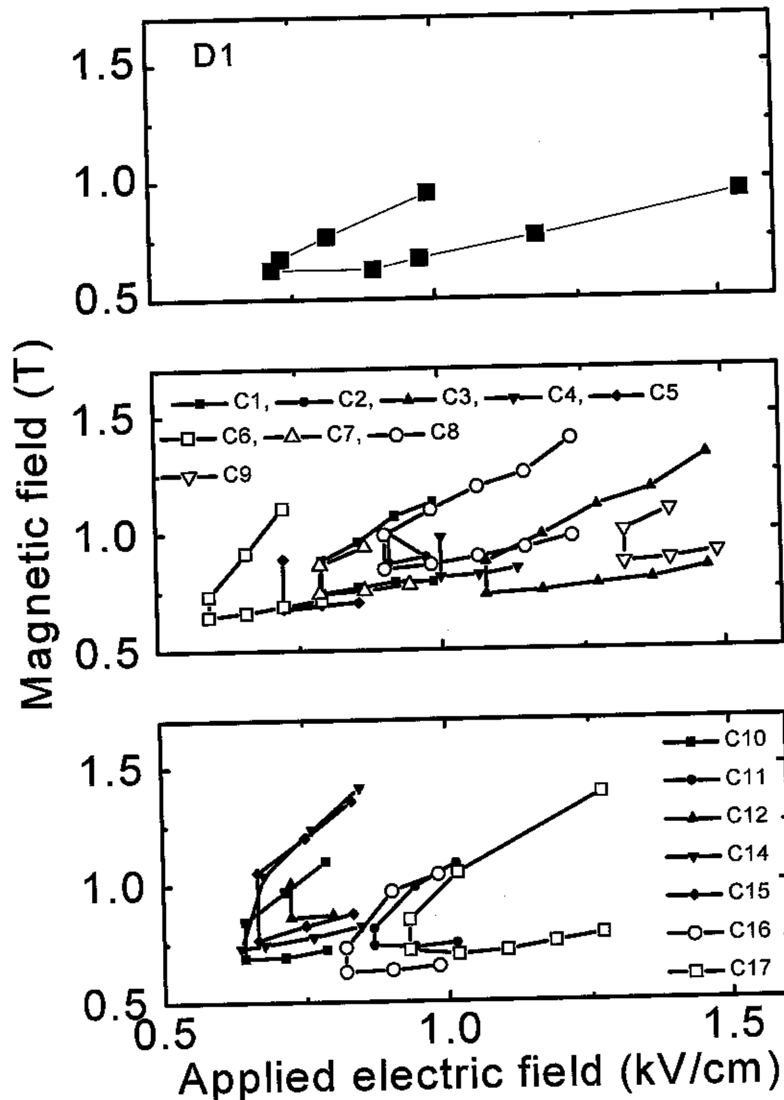

Fig. 9. (top) Zone for observed far infrared laser emission for annealed NTD laser rod D1 in applied field space. (middle) Laser generation zones of traditional melted samples C1-C12 and (bottom) C14-C17.

Far-infrared laser emission from NTD laser crystal D1 was observed after annealing. The region of observed laser emission in the space of applied electric and magnetic fields is plotted in Fig. 9. The electric field threshold is comparable to the lowest thresholds found in melt-doped material C, but the current density threshold is considerably lower at 50.7 A/cm^2.

Saturated current density vs. electric field applied via lateral laser contacts was measured for D1 and C6 in liquid helium. For a given crystal, saturation curves for different applied magnetic fields asymptotically approach the same saturated current density J_s. Using Eq. 5, hole concentrations p are determined from J_s values and plotted against normalized gallium concentration from NAA as open symbols in Fig. 10. Values of p determined from resistivity data and Eq. 4 are plotted as solid symbols in Fig. 10. The crystal D1 has a lower hole concentration than C6 by a factor 1.04 (resistivity data) to 1.5 (current saturation data). Since the Ga concentration of D1 is higher, its compensation is higher. By calibrating the concentration scale using p, the expected compensation of 32-40% for D1, and Eq. (6), lines of zero compensation (or p = [Ga]) can be drawn. The straight line in Fig. 6 is the K=0 line found using the p values from resistivity data and a K value of 32% for D1.

This suggests that the compensation of the C6 crystal is ~20%. If K was set to 40% for D1, the compensation of C6 would be ~30%. Hence, the NTD laser crystal has compensation 1.3 to 1.6 times higher than the best of the melt-doped crystals studied.

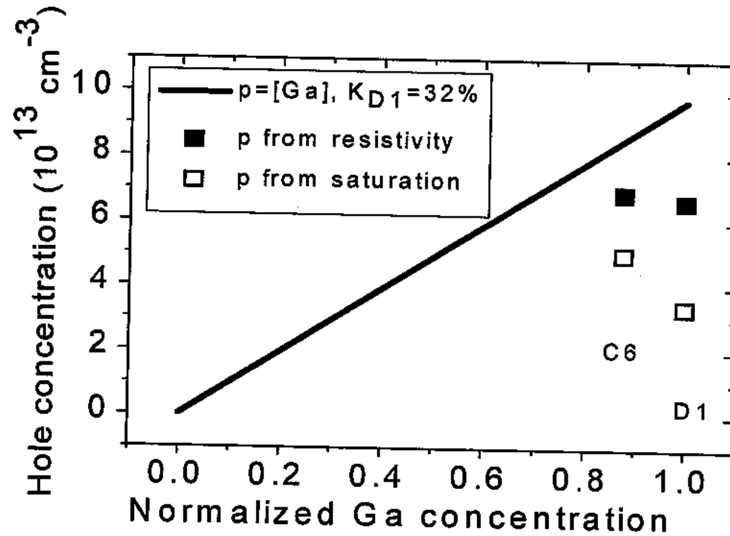

Fig. 10. Hole concentration p as a function of normalized Ga concentration for melt-doped crystal C6 and for annealed NTD crystal D1 as determined by room temperature resistivity (solid symbols) and as determined by saturation current density at 4 K (open symbols). The zero compensation line is found by calibrating the normalized concentration using the D1 p value from resistivity and assuming 32% compensation.

Current saturation curves were compared for rods of material C and annealed (1 hr at 390 C) material D having identical geometry and axial current flow (Fig.11). The transition to saturation is slightly sharper for the NTD crystal than for the melt-doped crystal. The difference is less than the simulated Fig. 7 curves, though it was expected that real crystals would have less extreme inhomogeneity than the simulation model used for Fig. 7. Nevertheless, these data support the assertion that the doping uniformity achieved in the NTD crystal is higher than in the melt-doped crystal studied.

DISCUSSION

Electric field threshold of the laser operation is a qualitative indicator of laser gain. Thus, Fig. 5 indicates a large variation in the quality of laser rods prepared from the same melt-doped boule and tested under identical conditions. This variability can be attributed to the poor uniformity of low-concentration doping for melt-doped crystals. Since most of the best performing crystals tend to come from the same portion of each hemi-cylinder (Fig. 8), there is likely substantial doping inhomogeneity over cm length scales. Hence, a typical melt-doped p-Ge boule will have low yield of good laser rods.

Current density threshold for D1 is a factor 1.5 times smaller than found for the best of the C crystals (C6). This positive result occurs despite a much smaller active volume for D1. The larger number of round trips required to build up laser oscillation therefore implies that the low D1 threshold occurs despite higher output coupling, mirror loss, and other potential electrodynamic losses. The NTD p-Ge laser material was found to be a factor 1.3 to 1.6 times more highly compensated than the best of the melt-doped crystals studied for comparison. Nevertheless, the current density threshold for lasing was found to be considerably lower in the NTD crystal. This observation is consistent with the prediction from Monte Carlo calculations (Fig. 6) that compensation has little negative effect at hole concentration 3.6×10^{13} cm^{-3} (the value for the NTD laser crystal tested.)

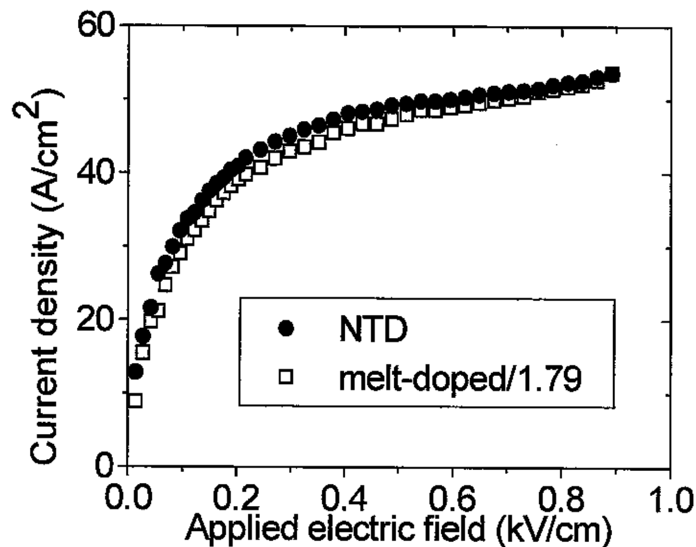

Fig. 11. Current density vs. applied electric field for annealed NTD (D) and melt-doped (C) p-Ge crystals of identical dimensions. A small longitudinal magnetic field of 0.19 T is applied to suppress electron injection. Sample temperature was 4 K. The data are scaled to have the same maximum value. The scaling factor is given in the legend.

A controllable, repeatable process such as NTD should allow higher yield of good laser rods per kg of material. Given current prices for melt-doped (~$3/g) and ultra-high purity Ge crystals (~$5/g), the yield need only be twice better to make NTD economically preferable. The neutron-irradiation fee at UFTR is $100/hour, which is negligible compared with other costs of producing a commercial p-Ge laser (primarily cryogenics and specialized electronics). Residual radiation is equivalent to background, so properly aged NTD Ge poses no health risk. High-purity Ge starting material for NTD is commercially available while suitable melt-doped Ge is not a standard commercial item.

SUMMARY AND CONCLUSIONS

A far-infrared p-Ge laser with neutron transmutation doped active crystal was demonstrated. A high degree of uniformity for the Ga-acceptor distribution, easily obtained by NTD, but unusual in melt-doped Ge, was shown to be important for p-Ge laser operation. Current saturation behavior supports the expected higher homogeneity for

this doping process. Despite the negative factor of higher compensation, this first un-optimized NTD p-Ge laser achieves a current density threshold significantly smaller than the best of 18 melt-doped lasers studied for comparison. Optimization of the NTD process should eventually permit smaller rods with lower thresholds, increased gain, and higher duty cycles.

Table 3. Laser rods. Material C is melt doped. Material D is neutron transmutation doped. An asterisk (*) designates non-working lasers. The dimensions given are the long axis (B-field direction), E-field direction, and direction perpendicular to E, respectively. Crystallographic orientations are [110] x [-110] x [001] for these directions for all crystals.

Designation	Dimensions [mm^3]	E-field lasing threshold (kV/cm)
C1	51.8 x 7.6 x 5.1	0.78
C2	51.2 x 7.5 x 5.2	0.91
C3	51.8 x 7.6 x 5.1	1.1
C4	51.3 x 7.5 x 5.1	1.0
C5	51.2 x 7.6 x 4.2	0.72
C6	51.2 x 7.6 x 3.65	0.64
C7	51.2 x 6.35 x 4.0	0.78
C8	51.8 x 6.1 x 5.0	0.90
C9	51.8 x 6.05 x 4.75	1.3
C10	45.45 x 7.0 x 3.2	0.86
C11	45.45 x 6.95 x 3.1	0.86
C12	45.45 x 6.0 x 2.5	0.72
* C13	45.45 x 6.9 x 3.1	-
C14	45.7 x 5.9 x 2.6	0.64
C15	45.7 x 6.0 x 2.5	0.67
C16	45.7 x 6.1 x 2.85	0.82
C17	45.7 x 5.9 x 2.51	0.93
* C18	45.7 x 5.9 x 4.3	-
D1	17.40 x 6.16 x 2.44	0.71

ACKNOWLEDGMENTS

This work was partially supported by the National Science Foundation (ECS0070228), by a BMDO SBIR Phase I (administered by US Army SMDC, DASG60-01-P-0043), and by an AFOSR STTR Phase II (F49620-02-C-0027).

REFERENCES

1. E. Bründermann , "Widely tunable far-infrared hot hole semiconductor lasers" in *Long Wavelength Infrared Semiconductor Lasers* edited by H.K.Choi (Wiley, NY, 2004) Chap.6.
2. Shlimak, *Physics of the Solid State* **41**, 716 (1999).
3. H. Fritzsche and M. Cuevas, *Physical Review* **119**, 1238 (1960).
4. K. M. Itoh, E. E. Haller, W. L. Hansen, J. W. Beeman, J. W. Farmer, A. Rudnev, A. Tikhomirov, and V. I. Ozhogin, *Appl. Phys. Lett.* **64**, 2121 (1994).
5. E. W. Nelson, E. S. Flitsiyan, A. V. Muravjov, M. V. Dolguikh, R. E. Peale, S. H. Kleckley, W. G. Vernetson, and V. Z. Tsipin, in *High-Power Fiber and Semiconductor Lasers*, edited by M. Fallahi and J. V. Maloney, Proc SPIE v. **4883**, 10 (2003).
6. E. W. Nelson, M. V. Dolguikh, E. S. Flitsiyan, A. V. Muravjov, R.E. Peale, S. H. Kleckley, W. G. Vernetson, and V. Z. Tsipin, in *Laser Systems Technology*, edited by W. E. Thompson and P. H. Merritt, Proc. SPIE v. **5087**, 133 (2003).
7. E. Bründermann, Ruhr University, Bochum, Germany, private communication, December 9, 2002.
8. L. E. Vorobjev, S. N. Danilov, V. I. Stafeev, *Opt. Quantum Electron.* **23**, S195 (1991).
9. M. V. Dolguikh, A. V. Muravjov, and R. E. Peale, in *Novel in-plane semiconductor lasers III*, edited by C.F.Gmachl and D. P. Bour, Proc. SPIE v. **5365** (2004).
10. R. C. Strijbos, J. G. S. Lok, and W. T. Wenckebach, *J. Phys. Condens. Matter* **6**, 7461 (1994).

Author Index

Abreu, Rene, 25
Barat, Robert, 9, 45
Bosacchi, Bruno, 92
Cao, Hua, 150
Ceperley, Peter H., 174
Cerne, John, 182
Chen, Caihua, 116
Chen, Jing-Yin, 182
Chen, Yunqing, 1
Cheville, R. Alan, 196
Cox, William A., 182
Cunningham, Nicholas, 136
Deng, Yanqing, 1
Dodson, Caroline, 1, 84
Dolguikh, Maxim V., 207, 216
Du Bosq, Todd W., 167, 216
Ediss, Geoff, 25
Erickson, Joshua, 136
Federici, John F., 9, 45
Fitch, Michael J., 1, 84
Flitsiyan, Elena S., 216
Foshee, James F., 174
Fredricksen, Christopher J., 158, 216
Gary, Dale, 9, 45
Globus, Tatiana, 25
Grischkowsky, Daniel R., 196
Gross, Mike, 136
Grossman, Erich N., 18, 68, 121
Hadfield, Robert H., 121
Hagmann, Mark J., 51
Hagmann, Zulaima S., 51
Hesler, Jeffrey L., 25
Huang, Feng, 45
Jedju, Thomas M., 92
Joung, Minkyoo, 99
Kagaya, Shunichi, 99
Karpowicz, Nick, 33
Khromova, Tatyana, 25
Knab, Joseph R., 182
Kuenstner, Todd, 92
Lin, Chunchen, 116
Liu, Haibo, 1
Lu, Zhaolin, 116
Luukanen, Arttu, 18, 68, 121
Majewski, Alexander, 25
Manning, Christopher J., 136
Markelz, Andrea G., 182
Matono, Haruki, 99
McBride, B. A., 51
Meyer, Jerry R., 187
Miller, Aaron J., 18, 68, 121
Mizuno, Koji, 99
Muravjov, Andrei V., 158, 167, 207, 216
Nahata, Ajay, 92, 150
Nelson, Eric W., 216
O'Hara, John, 196
Oliveira, Filipe, 45
Osiander, Robert, 1, 84
Pan, Shing-Kuo, 25
Partasarathy, Ramakrishnan, 25
Partridge, Jason, 33
Peale, Robert E., 158, 167, 207, 216
Prather, Dennis W., 116
Reiten, Matthew T., 196
Samuels, Alan C., 136
Schauki, Dunja, 1, 84
Schneider, Garrett J., 116
Schulkin, Brian, 9, 45
Seminario, Jorge M., 103
Shur, Michael S., 1
Spicer, James B., 1
Suzuki, Yusuke, 99
Tanaka, Terukazu, 99
Veksler, Dmitry B., 1
Velazco, Jose E., 174
Vernetson, William G., 216
Wagatsuma, Yoshihiko, 99
Walsh, Kenneth P., 9
Warren, Warren S., 92
Watanabe, Keisuke, 99
White, Jeffrey S., 78
Wiltse, James C., 127
Woolard, Dwight L., 25
Wu, Dong Ho, 187
Xie, Xu, 33
Xu, Jingzhou, 33
Zhang, Xi-Cheng, 1, 33
Zhong, Hua, 33
Zimdars, David, 9, 45, 78